

Structural basis of charge transfer complex formation by riboflavin bound to 6,7-dimethyl-8-ribityllumazine synthase

Michael Koch¹, Constanze Breithaupt¹, Stefan Gerhardt^{1,*}, Ilka Haase², Stefan Weber³, Mark Cushman⁴, Robert Huber¹, Adelbert Bacher² and Markus Fischer²

¹Abteilung Strukturforschung, Max-Planck-Institut für Biochemie, Martinsried, Germany; ²Lehrstuhl für Organische Chemie und Biochemie, Technische Universität München, Garching, Germany; ³Institut für Experimentalphysik, Freie Universität Berlin, Germany; ⁴Department of Medicinal Chemistry and Molecular Pharmacology, Purdue University, West Lafayette, IN, USA

The amino acid residue tryptophan 27 of 6,7-dimethyl-8-ribityllumazine synthase of the yeast *Schizosaccharomyces pombe* was replaced by tyrosine. The structures of the W27Y mutant protein in complex with riboflavin, the substrate analogue 5-nitroso-6-ribitylamino-2,4(1*H*,3*H*)-pyrimidin-2(1*H*)-edione, and the product analogue 6-carboxyethyl-7-oxo-8-ribityllumazine, were determined by X-ray crystallography at resolutions of 2.7–2.8 Å. Whereas the indole system of W27 forms a coplanar π -complex with riboflavin, the corresponding phenyl ring in the W27Y mutant establishes only peripheral contact with the heterocyclic ring system of the

bound riboflavin. These findings provide an explanation for the absence of the long wavelength shift in optical absorption spectra of riboflavin bound to the mutant enzyme. The structures of the mutants are important tools for the interpretation of the unusual physical properties of riboflavin in complex with lumazine synthase.

Keywords: biosynthesis of riboflavin; crystallization; 6,7-dimethyl-8-ribityllumazine synthase; mutagenesis; riboflavin binding.

The biosynthesis of vitamin B₂ (riboflavin) in eubacteria and fungi has been studied in considerable detail [1,2]. In brief, GTP cyclohydrolase II affords 2,5-diamino-6-ribosylamino-4(3*H*)-pyrimidinone. Reduction of the ribose side chain, deamination and dephosphorylation afford 5-amino-6-ribitylamino-2,4(1*H*,3*H*)-pyrimidin-2(1*H*)-edione (**1**), which is converted into 6,7-dimethyl-8-ribityllumazine (**3**) by condensation with 3,4-dihydroxy-2-butanone 4-phosphate (**2**) obtained from ribulose 5-phosphate by a sigmatropic migration of the terminal phosphoryl carbinol group and elimination of formate (Fig. 1).

6,7-Dimethyl-8-ribityllumazine synthase (lumazine synthase) catalyses the formation of the direct precursor of vitamin B₂ [3]. The lumazine synthases from yeasts and fungi are C₅-symmetric homopentamers [4–7], whereas plants and many bacteria form lumazine synthases of 60 identical subunits with icosahedral 532 symmetry [7–11]. The three-dimensional structures of these hollow, icosahedral particles are best described as dodecamers of pentamers. The subunit fold of all lumazine synthases that have been reported is very similar. A central four-stranded β -sheet is flanked on both

sides by two α -helices. The active sites of lumazine synthases are invariably located at each respective interface between adjacent subunits in the pentamer modules.

The binding of substrate and product analogues has been studied with the lumazine synthases of *Aquifex aeolicus*, *Magnaporthe grisea*, *Saccharomyces cerevisiae*, *Schizosaccharomyces pombe* and *Spinacia oleracea* [5–7,9]. Analogues of **1** and **3** are invariably bound via their ribityl side chain in an extended conformation.

Surprisingly, the pure enzyme of *S. pombe* shows an intense yellow colour after purification with a ratio of 6 : 1 of riboflavin/6,7-dimethyl-8-ribityllumazine bound in the active site, due to the relatively high affinity of the enzyme for the final product of the biosynthetic pathway.

In the wild-type enzyme of *S. pombe*, the heterocyclic moieties of various ligands, including riboflavin, have been shown to form coplanar π -complexes with the indole ring of tryptophan 27 [5]. In general, such π -stacking interactions are known to play an important role in the modulation of cofactor reactivities [12–16]. An example is found in flavodoxins, which utilize a flavin mononucleotide molecule as a cofactor in a highly conserved binding site containing tryptophan and tyrosine residues [17,18]. Coordination of flavin mononucleotide in a π -stacked configuration with these aromatic amino acid side chains stabilizes the oxidized redox state of the flavin cofactor and appears to disfavour the formation of the electron rich hydroquinone form. Furthermore, π -stacking interactions play a role in protein binding of flavins. For example, in the recently discovered flavoprotein dodecin, a pair of tryptophans facilitates the formation of a unique tetrad comprising of a pair of riboflavins with an antiparallel staggering of their isoalloxazine moieties, sandwiched by the indole groups of the symmetry-related tryptophans [19].

Correspondence to M. Fischer, Lehrstuhl für Organische Chemie und Biochemie, Technische Universität München, Lichtenbergstr. 4, D-85747 Garching, Germany. Fax: +49 89 28913363, Tel.: +49 89 28913336, E-mail: markus.fischer@ch.tum.de

Abbreviations: CEOL, 6-carboxyethyl-7-oxo-8-ribityllumazine; NORAP, 5-nitroso-6-(D-ribitylamino)-2,4(1*H*,3*H*)-pyrimidin-2(1*H*)-edione; NRAP, 5-nitro-6-(D-ribitylamino)-2,4(1*H*,3*H*)-pyrimidin-2(1*H*)-edione.

*Present address: AstraZeneca, Alderley Park, Macclesfield, SK10 4TG, UK.

(Received 26 March 2004, revised 7 June 2004, accepted 11 June 2004)

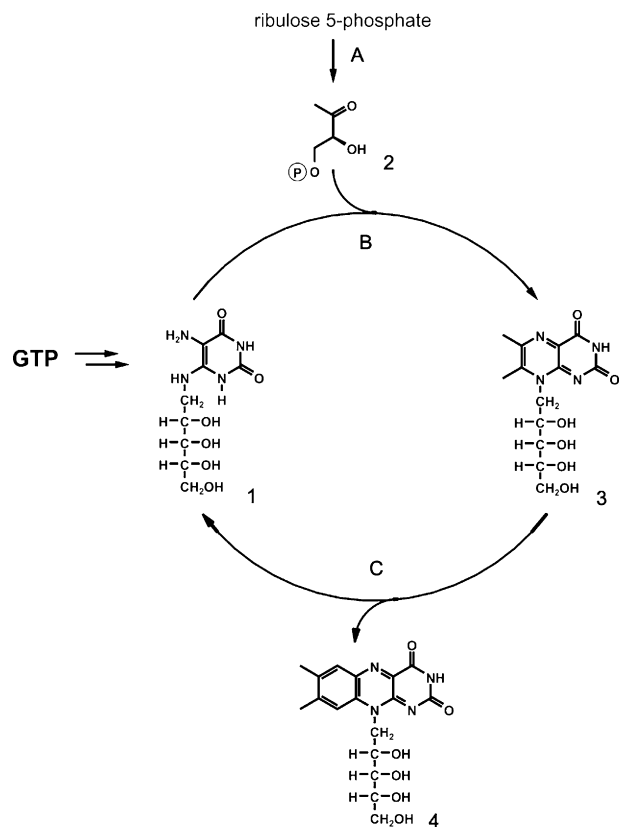


Fig. 1. Terminal reactions in the pathway of riboflavin biosynthesis. (A) 3,4-dihydroxy-2-butanone 4-phosphate synthase; (B) 6,7-dimethyl-8-ribytyllumazine synthase; (C) riboflavin synthase; 1, 5-amino-6-ribytylamino-2,4(1*H*,3*H*)-pyrimidinedione; 2, 3,4-dihydroxy-2-butanone 4-phosphate; 3, 6,7-dimethyl-8-ribytyllumazine and 4, riboflavin.

In the lumazine synthase, such a π -stacked topology correlates with a substantially modified optical absorption spectrum of bound riboflavin. Specifically, the absorbance of the protein-bound vitamin extends to wavelengths above 500 nm, and the relative intensity of the optical transitions at 445 and 370 nm is inverted compared to free riboflavin in aqueous solution. These features are less pronounced in a W27Y mutant and virtually absent in a W27G mutant of the protein [20]. Evidence for π -stacking interactions of W27 or other aromatic amino acid residues such as tyrosine and phenylalanine at the respective position with riboflavin is also provided by time-resolved EPR experiments from which the triplet parameters of riboflavin are obtained ([21] and S. Weber, C. W. M. Kay, E. Schleicher, I. Hasse, M. Koch, R. Huber, A. Bacher & M. Fischer, unpublished results). The extent of π -orbital overlap influences the flavin triplet delocalization, which is reflected in the triplet zero-field splitting parameters. Riboflavin bound to wild-type and mutant lumazine synthases thus represents an ideal system to specifically study such π -stacking interactions of flavins in a protein environment.

In order to provide the structural basis for further studies of the physical properties of riboflavin in complex with lumazine synthase, we have determined the three-dimensional structures of the W27Y mutant protein complexed with riboflavin, 6-carboxyethyl-7-oxo-8-ribytyllumazine

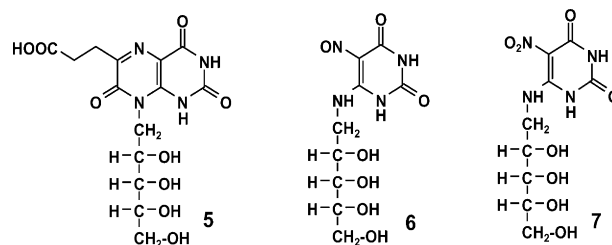


Fig. 2. Inhibitors of 6,7-dimethyl-8-ribytyllumazine synthase. 5, 6-Carboxyethyl-7-oxo-8-ribytyllumazine (CEOL), 6, 5-nitroso-6-(D-ribytylamino)-2,4(1*H*,3*H*)-pyrimidinedione (NORAP), and 7, 5-nitro-6-(D-ribytylamino)-2,4(1*H*,3*H*)-pyrimidinedione (NRAP).

(CEOL, 5; Fig. 2) and 5-nitroso-6-(D-ribytylamino)-2,4(1*H*,3*H*)-pyrimidinedione (NORAP, 6; Fig. 2) at resolutions of 2.80, 2.75 and 2.70 Å, respectively.

Experimental procedures

Materials

CEOL and NORAP were synthesized using published procedures [22,23]. Riboflavin was obtained from Sigma.

Protein purification and crystallization

The W27Y mutant of *S. pombe* lumazine synthase was cloned, expressed and purified as described previously [20]. After purification in the absence of riboflavin, less than 20% of the purified mutant protein contained bound riboflavin [5]. In order to obtain saturation with riboflavin, the protein was cocrystallised with riboflavin, and the crystals were subsequently soaked with riboflavin. Cocrystallization experiments with the substrate analogue NORAP and the product analogue CEOL were carried out by mixing purified mutant enzyme (11 mg·mL⁻¹) in 20 mM potassium phosphate (pH 7.0) and 50 mM potassium chloride with stock solutions of the inhibitors to a final 10-fold molar excess of the corresponding inhibitor. Crystals were grown at 18 °C by the sitting drop vapor diffusion method by mixing 2 μ L of the protein-inhibitor solution with 2 μ L of reservoir solution (0.1 M sodium citrate, pH 5.0, containing 0.7 M ammonium dihydrogen phosphate) and equilibrating against reservoir solution.

Data collection

X-ray data of the riboflavin-bound mutant enzyme W27Y as well as of the two inhibitor complex structures were collected on a MARRResearch (Norderstedt, Germany) 345 imaging plate detector system mounted on a Rigaku RU-200 rotating anode (Brandt Instruments, Prairieville, LA, USA) operated at 50 mA and 100 kV with $\lambda = \text{CuK}\alpha = 1.542 \text{ \AA}$. The data sets of the crystals that diffracted up to a resolution of 2.7 Å were integrated, scaled, and merged using the DENZO and SCALEPACK program packages [24]. Data collection statistics are shown in Table 1.

Structure solution and refinement

Initial phases of the riboflavin complex and the two inhibitor complexes were determined by difference Fourier

Table 1. X-ray data-processing and refinement statistics. RMSD, root mean square deviations of temperature factors of bonded atoms.

Data set	W27Y-riboflavin	W27Y-CEOL	W27Y-NORAP
Number of unique reflections	25 184	26 937	28 707
Multiplicity ^a	2.7 (2.1)	3.9 (3.8)	3.9 (3.8)
Limiting resolution (Å)	2.80	2.75	2.70
Completeness of data (%)	96.7 (91.6)	99.4 (99.5)	99.9 (100.0)
R _{merge} (%) ^b	8.5 (37.3)	8.0 (51.7)	10.9 (48.2)
I/σ	7.0 (2.0)	15.5 (2.6)	11.6 (2.6)
R _{cryst} /R _{free} (%) ^c	20.4/22.2	20.6/23.0	19.1/21.2
Non hydrogen protein atoms	5550	5550	5550
Number of water molecules	28	–	58
Non hydrogen ligand atoms	135	115	100
Non hydrogen ion atoms	25	25	25
RMSD [bonds (Å)/angles (°)/bonded Bs (Å ²)]	0.008/1.34/2.33	0.009/1.40/2.07	0.009/1.42/2.21
Mean temperature factors (protein/ligand/ion/solvent)	49.3/75.4/51.0/47.5	60.6/52.9/68.9/–	43.7/38.1/43.0/40.2

^a Values in parentheses correspond to the highest resolution shell between 2.95 and 2.80 Å (W27Y-riboflavin), 2.83–2.75 Å (W27Y-CEOL) and 2.78–2.70 Å (W27Y-NORAP). ^b $R_{\text{merge}} = \sum_h \sum_l |I_l(\mathbf{h}) - \langle I(\mathbf{h}) \rangle| / \sum_h \sum_l I_l(\mathbf{h})$. ^c $R_{\text{cryst}} = \sum_h ||F_o(\mathbf{h})| - |F_c(\mathbf{h})|| / \sum_h |F_o(\mathbf{h})|$.

synthesis using the lumazine synthase wild-type structure [5] as template. After initial rigid body minimization, refinement was performed by alternating model building carried out with the program o [25] and crystallographic refinement using CNS [26]. The refinement procedure included positional refinement and restrained temperature factor refinement. Finally, water molecules were inserted automatically and checked manually by inspection of the $F_o - F_c$ map. For all three models, noncrystallographic symmetry restraints were applied. The ligands were not included in the model during the first cycles of refinement; thereafter CEOL and NORAP could be easily built into the clearly defined electron density in contrast to riboflavin, which, due to its low occupancy, exhibited only weak electron density. Due to disorder, residues 159 and the N-terminal residues 1–12 remained undetermined in the electron density map. Stereochemical parameters of the structures were calculated with PROCHECK [27]. Figures were designed with MOLSCRIPT [28], BOBSCRIPT [29] and RASTER3D [30].

Results and discussion

In contrast to lumazine synthases from other organisms studied [6–8, 11], the enzyme from *S. pombe* binds riboflavin with relatively high affinity. This is believed to be due to a π -complex formation between the bound ligand and the adjacent tryptophan residue 27 [20]. In mutant proteins, namely W27Y and W27F, riboflavin is less tightly bound as compared to the wild-type protein. The three W27Y mutant lumazine synthase structures in complex with riboflavin, CEOL and NORAP were solved by difference Fourier synthesis using the coordinates of the riboflavin-bound wild-type structure from *S. pombe*. After refinement, more than 90% of the residues lie in the most favoured region of the Ramachandran plot in all three structures.

Crystals containing riboflavin belong to the space group C222₁ with unit cell constants $a = 111.6$ Å, $b = 145.1$ Å, $c = 129.2$ Å. The asymmetric unit contained one pentamer (Fig. 3). Crystals of the inhibitor complexes belong to the same space group with cell dimensions of $a = 111.1$ Å,

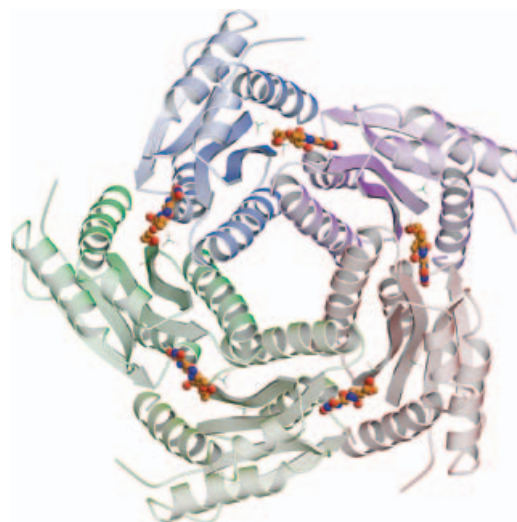


Fig. 3. Overall X-ray structure of W27Y mutant 6,7-dimethyl-8-ribityllumazine synthase – the pentameric assembly. Pentameric assembly of the 6,7-dimethyl-8-ribityllumazine synthase mutant W27Y from *S. pombe*. The inhibitor CEOL is shown as a ball-and-stick model. Subunits: A, red; B, light green; C, green; D, blue; E, violet.

$b = 144.9$ Å, $c = 128.3$ Å (CEOL) and $a = 111.2$ Å, $b = 144.8$ Å, $c = 127.8$ Å (NORAP), respectively. The monomers of *S. pombe* lumazine synthase consist of 159 residues that were well defined in all structures with the exception of residue 159 and the N-terminal residues 1–12 that remained undetermined in the electron density map (Fig. 4).

The five active sites of lumazine synthase are located at the interfaces between each adjacent pair of monomers (Fig. 3). Thus, residues of two adjacent monomers contact the ligands that bind into the substrate binding pocket. Y27, H94 and W63 of one monomer form most of the substrate binding site, and L119 and H142 of the second monomer close the pocket from the opposite side (Figs 5 and 6).

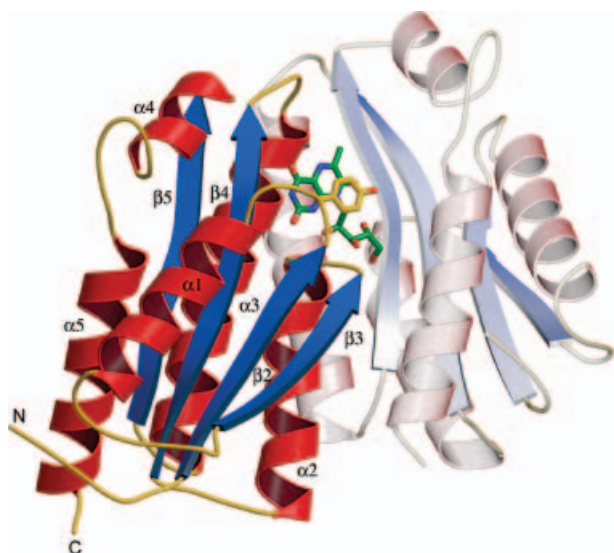


Fig. 4. Secondary structure arrangement of one lumazine synthase monomer and one neighbouring monomer (shown in lighter colours). At the subunit interface, in the active site, the inhibitor CEOL (green) and the mutated W27 residue (yellow) are shown.

Comparing the different wild-type and W27Y structures in complex with the different ligands, significant changes of the side chain conformation are observed for residue H94 (Fig. 7). H94 is highly conserved in all known lumazine synthase sequences and is assumed to be involved in the initial proton transfer steps of catalysis [9]. The orientation of H94 varies according to the bound ligand but is nearly independent of the nature of residue 27. In the case of the two substrate analogue complexes of the wild-type and the W27Y mutant proteins, H94 is moved closer to the plane of the ligand, NORAP (6; Fig. 2) in the W27Y-mutant protein and 5-nitro-6-(D-riboitylamino)-2,4(1*H*,3*H*)-pyrimidinedione (NRAP) (7; Fig. 2), in the wild-type enzyme (distance between the C₇-atom of H94 and the N5-atom of

N(O)RAP: wild-type enzyme: 5.5 Å; W27Y mutant: 5.5 Å) than in the two corresponding complexes with the larger product analogue CEOL (5; Fig. 2) comprising two annealed 6-membered rings (distance between the C₇-atom of H94 and the N7-atom of CEOL: wild-type enzyme: 6.5 Å; W27Y mutant: 6.1 Å).

The smallest distance between the C₇-atom of H94 and the inhibitor plane (N5-atom of riboflavin) is found in the wild-type structure with bound riboflavin with a value of 4.9 Å. Moreover, the imidazole ring of H94 is packed nearly parallel against the riboflavin, contributing to the observed stacking interactions between the sandwiched riboflavin and H94 and residue 27 (distances between the planes of about 4 Å) [5].

In the CEOL and NORAP structures of the W27Y mutant and in all three ligand-bound structures of the wild-type enzyme [5], the positions of the C_α-atoms and the aromatic planes of residues Y27 and W27, respectively, are almost identical (distance between the ring system of the ligand and the aromatic planes of amino acid 27: 3.5 Å [5], Fig. 7). In the W27Y mutant structure with bound riboflavin, however, the C_α-trace deviates from the other structures by 0.6 Å, and the aromatic ring is very flexible. In the substrate and product analogue complexes of the mutant and the wild-type protein, stacking interactions take place between the ligand and Y27 or W27, respectively. This leads to a fixed orientation of the Y27 side chain, parallel to the ligand ring system with well defined electron densities for these two ligands (Figs 5 and 6). The ribityl side chain is bound in the same manner as already described for the *S. pombe* wild-type structure [5]. The mutant protein binds riboflavin less tightly (K_d : 12.0 μM [20]); as compared to the wild-type protein (K_d : 1.2 μM [20]); (for optical properties see [20]). The bound riboflavin in complex with the mutant protein is less well defined than the two other ligands and thus, its position cannot be determined reliably. This prevents aromatic stacking and thus the fixation of Y27.

For the *S. pombe* wild-type enzyme, a significant long-wavelength optical absorbance extending well beyond

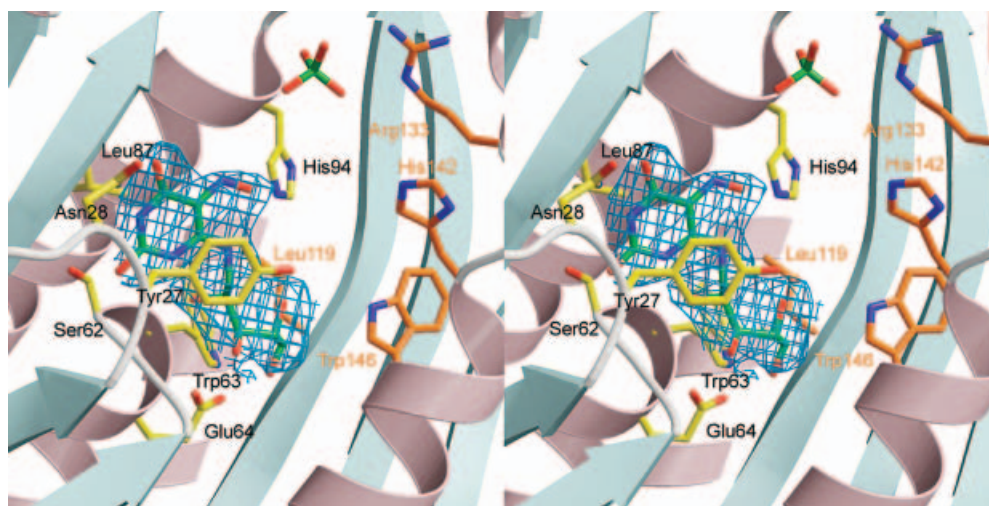


Fig. 5. Stereo view of the active site of W27Y 6,7-dimethyl-8-riboityllumazine synthase from *S. pombe* with bound substrate analogue NORAP (green) in the active site. The final (2*F_o*-*F_o*)-omit map of the inhibitor was calculated at 2.7 Å resolution.

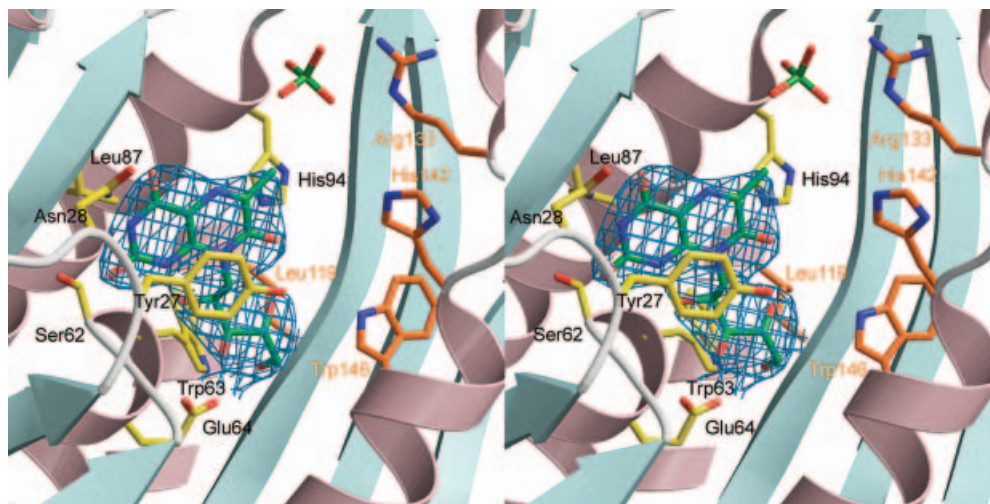


Fig. 6. Stereo view of the active site of W27Y 6,7-dimethyl-8-ribityllumazine synthase from *S. pombe* with bound product analogue CEOL (green) in the active site. The final ($2F_o - F_c$)-omit map of the inhibitor was calculated at 2.8 Å resolution.

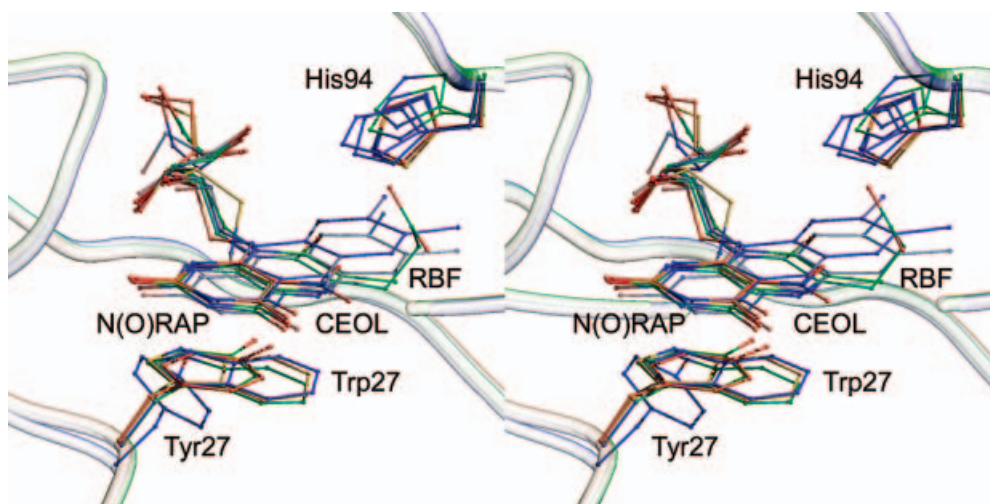


Fig. 7. Stereo drawing of the active sites of the wild-type and W27Y mutant 6,7-dimethyl-8-ribityllumazine-synthase-ligand complexes from *S. pombe*. CEOL complexes are shown in green for the W27Y mutant and in cyan for the wild-type enzyme, substrate analogue complexes in orange for the W27Y mutant with bound NORAP and in yellow for the NRAP-bound wild-type enzyme, the riboflavin-bound enzymes are shown in blue (mutant) and violet (wild-type), respectively. The position of residue H94 changes according to the bound ligand, independently of the nature of residue 27. The positions of the aromatic planes of the residues Y27 and W27 are almost identical for five of the six structures. The C_α -position of Y27 in the riboflavin-bound mutant enzyme differs from the position of residue 27 in the other proteins.

500 nm has been observed [20]. This feature is much less pronounced in the W27Y mutant. One possible reason for this finding is that the phenyl ring of Y27 in the mutant is rotated such that the coplanarity of its π -system and that of the riboflavin's isoalloxazine ring is reduced, whereas in the wild-type enzyme the aromatic rings W27 and riboflavin are almost perfectly coplanar. Nearly perfect π -stacking interactions between a tyrosine residue and a flavin have been observed, for example, in flavodoxin from *Desulfovibrio vulgaris* [31]. However no extended long-wavelength optical absorption has been found in that system [32]. Taking together these observations with our results, we conclude that the absence of long-wavelength absorption in the W27Y mutant of *S. pombe* lumazine synthase is not due to

the different orientation of the Y27's phenyl ring but rather due to the reduced π -orbital overlap as a consequence of the smaller size of the phenyl ring of Y27 as compared to the indole ring of W27. Clearly further biophysical studies are required to substantiate these notions.

The crystal structure of the lumazine synthase from *A. aeolicus* was the first structure without any ligand in the active site [8]. The superpositions of the amino acid residues in the active site of the *A. aeolicus* enzyme with the ones of the wild-type and the mutant enzyme of *S. pombe* in Fig. 8 shows that the phenyl ring of residue F22 in the *A. aeolicus* enzyme is rotated by 30° as compared to the orientation of the aromatic residue in W27 in the *S. pombe* wild-type enzyme, for which coplanarity between the aromatic planes

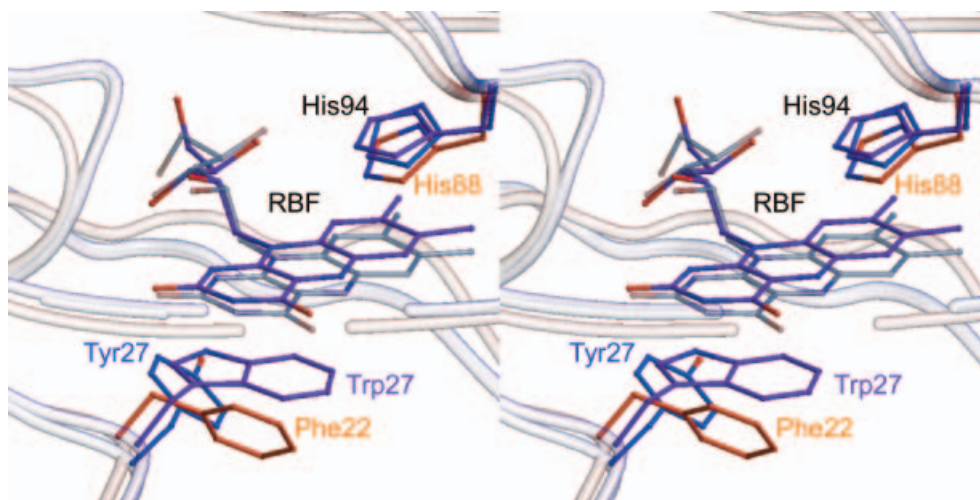


Fig. 8. Stereo view of the active sites of the *S. pombe* 6,7-dimethyl-8-ribityllumazine synthase W27Y mutant complexed with riboflavin (blue), the *S. pombe* 6,7-dimethyl-8-ribityllumazine synthase wild-type enzyme complexed with riboflavin (violet) and the *A. aeolicus* lumazine synthase with no bound ligand (orange). The residue F22 from *A. aeolicus* has an orientation 30° bent to the orientation of W27 in the *S. pombe* wild-type enzyme, which is coplanar to the aromatic plane of bound aromatic ligands [9]. The orientation of Y27 in the *S. pombe* W27Y mutant resembles the *A. aeolicus* apoprotein more closely than the *S. pombe* wild-type enzyme complex. This relates to the higher dissociation constant in the riboflavin–mutant complex compared to the riboflavin–wild-type complex.

of the aromatic ligand is observed [9]. The orientation of residue Y27 in the *S. pombe* W27Y mutant is not coplanar to the aromatic plane (see above). Furthermore, the position of the indole ring of W27 in the wild-type enzyme is not fixed after elimination of riboflavin. Hence, it can be concluded that the orientation of Y27 in the mutant resembles the situation in the protein without ligand. This is the reason for the lower content of riboflavin in the riboflavin–mutant complex compared to the riboflavin–wild-type complex.

The interaction of the N-terminal residue P8 with W27 in the wild-type complex is missing in the mutant complex where the N-terminal region is not defined in the electron density. The π – π -stacking interaction between the aromatic residue 27 and the pyrimidine system presumably contributes substantially to the substrate-binding energy [9]. Here, this binding energy is expected to be lowered, leading to a reduced affinity for the ligand.

The residue H142 shows a smaller, but still recognizable deviation in the two structures with bound riboflavin as compared to the structures with other bound inhibitors. H142 is assumed to form a salt bridge to the phosphate ion of the second substrate, 3,4-dihydroxy-2-butanone-4-phosphate, during catalysis and is itself stabilized in its position by D145 [9]. In the substrate and product analogue complexes, a phosphate ion is bound to the phosphate binding site of the second substrate [5] that exhibits no direct contact with the substrate and product analogues. The much larger riboflavin, which is intuitively supposed to be unable to bind into the pocket, moves the position of H142 with respect to the other bound ligands.

Our findings clearly demonstrate that W27 in the wild-type enzyme plays an essential role in substrate fixation by π -orbital overlap of the indole ring of W27 with the aromatic ring(s) in the substrate. The different extent of π – π interaction mediated by residue 27 in the wild-type and in various mutants (W27Y, W27F, W27H) correlates favorably with

the different amounts of riboflavin specifically bound to the protein [20]. Furthermore, the parallel alignment of the isoalloxazine ring of riboflavin and the aromatic side chain of residue 27 in lumazine synthase manifests itself in the unusual spectral properties of the wild-type and mutant complexes indicating that partial π – π charge transfer between the rings has taken place even in the ground state. Stacking interactions are a well known structure motif in flavoproteins but also, for example, in riboflavin analogues in the solid state [33,34] where the intimate overlap of the isoalloxazine core provides an energetically favored packing mode. That this ring stacking can be manipulated by specific site-selective mutagenesis makes the lumazine synthase an ideal model system for studying flavin-binding to proteins at a molecular level and thus may contribute to an understanding of the fundamentally different reaction mechanisms catalysed by flavoproteins.

Acknowledgements

We thank Richard Feicht, Sebastian Schwamb and Thomas Wojtulewicz for skillful help in protein preparation. This work was supported by the Deutsche Forschungsgemeinschaft, the Fonds der Chemischen Industrie, the Hans-Fischer-Gesellschaft e.V., and by NIH grant GM51469.

References

1. Bacher, A., Eberhardt, S., Eisenreich, W., Fischer, M., Herz, S., Illarionov, B., Kis, K. & Richter, G. (2001) Biosynthesis of riboflavin. *Vitamins Hormones* **61**, 1–49.
2. Bacher, A., Eberhardt, S., Fischer, M., Kis, K. & Richter, G. (2000) Biosynthesis of vitamin B₂ (Riboflavin). *Annu. Rev. Nutr.* **20**, 153–167.
3. Neuberger, G. & Bacher, A. (1986) Biosynthesis of riboflavin. Enzymatic formation of 6,7-dimethyl-8-ribityllumazine by heavy

- riboflavin synthase from *Bacillus subtilis*. *Biochem. Biophys. Res. Commun.* **139**, 1111–1116.
4. Braden, B.C., Vekilovsky, C.A., Cauerhff, A.A., Polikarpov, I. & Goldbaum, F.A. (2000) Divergence in macromolecular assembly: X-ray crystallographic structure analysis of lumazine synthase from *Brucella abortus*. *J. Mol. Biol.* **297**, 1031–1036.
 5. Gerhardt, S., Haase, I., Steinbacher, S., Kaiser, J.T., Cushman, M., Bacher, A., Huber, R. & Fischer, M. (2002) The structural basis of riboflavin binding to *Schizosaccharomyces pombe* 6,7-dimethyl-8-ribityllumazine synthase. *J. Mol. Biol.* **318**, 1317–1329.
 6. Meining, W., Mörtl, S., Fischer, M., Cushman, M., Bacher, A. & Ladenstein, R. (2000) The atomic structure of pentameric lumazine synthase from *Saccharomyces cerevisiae* at 1.85 Å resolution reveals the binding mode of a phosphonate intermediate analogue. *J. Mol. Biol.* **299**, 181–197.
 7. Persson, K., Schneider, G., Douglas, B.J., Viitanen, P.V. & Sandalova, T. (1999) Crystal structure analysis of a pentameric fungal and icosahedral plant lumazine synthase reveals the structural basis of differences in assembly. *Protein Sci.* **8**, 2355–2365.
 8. Zhang, X., Meining, W., Fischer, M., Bacher, A. & Ladenstein, R. (2001) X-ray structure analysis and crystallographic refinements of lumazine synthase from the hyperthermophile *Aquifex aeolicus* at 1.6 Å resolution: determinants of thermostability revealed from structural comparisons. *J. Mol. Biol.* **306**, 1099–1114.
 9. Zhang, X., Meining, W., Cushman, M., Haase, I., Fischer, M., Bacher, A. & Ladenstein, R. (2003) The catalytic mechanism of lumazine synthase. A structure based model of the reaction catalyzed by lumazine synthase from *Aquifex aeolicus*. *J. Mol. Biol.* **328**, 167–182.
 10. Ritsert, K., Huber, R., Turk, D., Ladenstein, R., Schmidt-Bäse, K. & Bacher, A. (1995) Studies on the lumazine synthase/riboflavin synthase complex of *Bacillus subtilis*: crystal structure analysis of reconstituted, icosahedral beta-subunit capsids with bound substrate analogue inhibitor at 2.4 Å resolution. *J. Mol. Biol.* **253**, 151–167.
 11. Ladenstein, R., Meyer, B., Huber, R., Labischinski, H., Bartels, K., Bartunik, H.D., Bachmann, L., Ludwig, H.C. & Bacher, A. (1986) Heavy riboflavin synthase from *Bacillus subtilis*. Particle dimensions, crystal packing and molecular symmetry. *J. Mol. Biol.* **187**, 87–100.
 12. Breinlinger, E.C., Keenan, C.J. & Rotello, V.M. (1998) Modulation of flavin recognition and redox properties through donor atom π -interactions. *J. Am. Chem. Soc.* **120**, 8606–8609.
 13. Breinlinger, E.C. & Rotello, V.M. (1997) Model systems for flavoenzyme activity. Modulation of flavin redox potentials through π -stacking interactions. *J. Am. Chem. Soc.* **119**, 1165–1166.
 14. Hunter, C.A. & Sanders, J.K.M. (1990) The nature of π - π interactions. *J. Am. Chem. Soc.* **112**, 5525–5534.
 15. Lostao, A., Gomez-Moreno, C., Mayhew, S.G. & Sancho, J. (1997) Differential stabilization of the three FMN redox forms by tyrosine 94 and tryptophan 57 in flavodoxin from *Anabaena* and its influence on the redox potentials. *Biochemistry* **36**, 14334–14344.
 16. Zhou, Z. & Swenson, R.P. (1996) The cumulative electrostatic effect of aromatic stacking interactions and the negative electrostatic environment of the flavin mononucleotide binding site is a major determinant of the reduction potential for the flavodoxin from *Desulfovibrio vulgaris* [Hildenborough]. *Biochemistry* **35**, 15980–15988.
 17. Vervoort, J., Muller, F., LeGall, J., Bacher, A. & Sedlmaier, H. (1985) Carbon-13 and nitrogen-15 nuclear-magnetic-resonance investigation on *Desulfovibrio vulgaris* flavodoxin. *Eur. J. Biochem.* **151**, 49–57.
 18. Stockman, B.J., Richardson, T.E. & Swenson, R.P. (1994) Structural changes caused by site-directed mutagenesis of tyrosine-98 in *Desulfovibrio vulgaris* flavodoxin delineated by 1H and 15N NMR spectroscopy: implications for redox potential modulation. *Biochemistry*, **33**, 15298–15308.
 19. Bieger, B., Essen, L.O. & Oesterhelt, D. (2003) Crystal structure of halophilic dodecin: a novel, dodecameric flavin binding protein from *Halobacterium salinarum*. *Structure* **11**, 375–385.
 20. Fischer, M., Haase, I., Feicht, R., Richter, G., Gerhardt, S., Changeux, J.P., Huber, R. & Bacher, A. (2002) Biosynthesis of riboflavin. 6,7-Dimethyl-8-ribityllumazine synthase of *Schizosaccharomyces pombe*. *Eur. J. Biochem.* **269**, 519–526.
 21. Schleicher, E., Kowalczyk, R.M., Kay, C.W.M., Hegemann, P., Bacher, A., Fischer, M., Bittl, R., Richter, G. & Weber, S. (2004) On the reaction mechanism of adduct formation in LOV domains of the plant blue light receptor phototropin. *J. Am. Chem. Soc.*, in press.
 22. Cushman, M., Yang, D., Gerhardt, S., Huber, R., Fischer, M., Kis, K. & Bacher, A. (2002) Design, synthesis, and evaluation of 6-carboxyalkyl and 6-phosphonoxyalkyl derivatives of 7-oxo-8-ribitylluminolumazines as inhibitors of riboflavin synthase and lumazine synthase. *J. Org. Chem.* **67**, 5807–5816.
 23. Plaut, G.W.E. & Harvey, R.A. (1971) The enzymatic synthesis of riboflavin. *Meth. Enzymol.* **18**, 515–538.
 24. Otwinowski, Z.M.W. (1993) *DENZO: A film-processing program for macromolecular crystallography*. Yale University Press, New Haven, CT.
 25. Jones, T.A., Zou, J.Y., Cowan, S.W. & Kjeldgaard, M. (1991) Improved methods for building protein models in electron density maps and the location of errors in these models. *Acta Crystallogr., Sect. A: Found. Crystallogr.* **47**, 110–119.
 26. Brunger, A.T., Adams, P.D., Clore, G.M., DeLano, W.L., Gros, P., Grosse-Kunstleve, R.W., Jiang, J.S., Kuszewski, J., Nilges, M., Pannu, N.S., Read, R.J., Rice, L.M., Simonson, T. & Warren, G.L. (1998) Crystallography & NMR system: a new software suite for macromolecular structure determination. *Acta Crystallogr., Sect. D: Biol. Crystallogr.* **54**, 905–921.
 27. Laskowski, R.A., MacArthur, M.W., Moss, D.S. & Thornton, J.M. (1993) PROCHECK – a program to check the stereochemical quality of protein structures. *J. Appl. Cryst.* **26**, 283–291.
 28. Kraulis, P.J. (1991) Molscript – a program to produce both detailed and schematic plots of protein structures. *J. Appl. Cryst.* **24**, 946–950.
 29. Esnouf, R.M. (1997) An extensively modified version of Molscript that includes greatly enhanced coloring capabilities. *J. Mol. Graph. Model.* **15**, 112–113.
 30. Merritt, E.A. & Murphy, M.E.P. (1994) Raster3d, Version 2.0 – a program for photorealistic molecular graphics. *Acta Crystallogr., Sect. D: Biol. Crystallogr.* **50**, 869–873.
 31. Walsh, M.A., McCarthy, A., O'Farrell, P.A., McArdle, P., Cunningham, P.D., Mayhew, S.G. & Higgins, T.M. (1998) X-ray crystal structure of the *Desulfovibrio vulgaris* (Hildenborough) apoflavodoxin-riboflavin complex. *Eur. J. Biochem.* **258**, 362–371.
 32. Dubourdieu, M., Le Gall, J. & Favaudon, V. (1975) Physicochemical properties of flavodoxin from *Desulfovibrio vulgaris*. *Biochim. Biophys. Acta* **376**, 519–532.
 33. Ebitani, M., In, Y., Ishida, T., Sakaguchi, K., Flippen-Anderson, J.L. & Karle I.L. (1993) Structures of riboflavin tetraacetate and tetrabutrylate – molecular packing mode of riboflavin tetracarboxylate and its extensive stacking and hydrogen-bonding characteristics. *Acta Crystallogr., Sect. A: Found. Crystallogr.* **49**, 136–144.
 34. Wang, M. & Fritchie, C.J.J. (1973) Geometry of the unperturbed flavin nucleus. The crystal structure of 10-methylisoalloxazine. *Acta Crystallogr., Sect. B* **29**, 2040–2045.